Tellus (2006), 58A, 368–384
Printed in Singapore. All rights reserved

TELLUS

Normal modes of an incompressible and stratified fluid model including the vertical and horizontal components of coriolis force

By AKIRA KASAHARA* and JOHN M. GARY, *National Center for Atmospheric Research, Boulder, Colorado, USA*

(Manuscript received 28 July 2005; in final form 26 October 2005)

ABSTRACT

Numerical solutions of the normal modes of a linearized Boussinesq fluid model are studied with respect to the variable static stability in height z, the Brunt-Väisälä frequency $N(z)$. The model includes both the vertical and horizontal components of Coriolis force. Our aim is to explore the characteristics of the little-known class of normal modes, referred to as the 'boundary-induced inertial (BII)' modes, in addition to the traditional inertio-gravity (IG) modes. Two kinds of finite-difference schemes are used to set up the eigenvalue-eigenvector matrix problem for crosscheck.

Numerical results of the characteristics of IG and BII modes are presented for the case of an exponential form of $N(z)$, together with the cases of constant N, whose exact solutions are used to check the performance of the numerical models. Because the frequencies of BII modes are close to the inertial frequency, which is a singular point of the model, the eigenfunctions of BII modes become highly oscillatory in z for a large value of N. It is shown that, under a realistic profile of $N(z)$ in the oceans, the BII modes can appear complementary to the IG modes throughout the domain, suggesting that the joint consideration of both the IG and BII modes is necessary to understand the near-inertial oscillations in the seas.

1. Introduction

The objective of this study is to contribute to our understanding of a little-known class of normal modes that emerge in atmospheric and oceanic numerical models, in addition to the well-known acoustic, inertio-gravity, and planetary (Rossby) modes, when the complete Coriolis forces arising from both the vertical and horizontal components of the Earth's rotation are included. This particular class of oscillation modes, whose frequencies are close to the inertial (Coriolis) frequency, are referred to here as the 'boundary-induced inertial (BII)' modes, because without the imposition of boundary conditions at the top and bottom of the system, this class of modes are absent.

The BII modes were recently rediscovered by Thuburn et al. (2002) and, independently, Kasahara (2003a,b) from the normal mode analysis of a compressible and stratified model on a tangent plane with complete rotation. Because of the assumption of constant Coriolis parameters, the planetary (Rossby) modes are not included in this consideration. What is unique about the emergence of the BII modes is that the linear system of equations that consists of five time-dependent variables gives rise to six eigenfrequencies with the imposition of solid boundary conditions at the bottom and top of the system. If the vertical boundary conditions are absent, the system yields only five eigenfrequencies associated with harmonic eigenfunctions. This rediscovery is at odds with the conventional notion that the system of five time-dependent equations that includes only the vertical component of the Earth's rotation yields at most five eigenfrequencies, including steady-state geostrophic relations with zero eigenfrequency, besides the external modes such as Lamb waves, which are not included in the number of internal-mode eigenfrequencies.

The emergence of the BII modes, however, is not directly connected to the compressibility of the system. The BII modes also appear in the homogeneous incompressible and Boussinesq models as long as both the vertical and horizontal components of rotation are included (Stern, 1975; Kamenkovich and Kulakov, 1977; Miropol'sky, 2001; Thuburn et al., 2002; Kasahara, 2003a,b; Durran and Bretherton, 2004). These studies deal with the normal mode analysis of linearized models in which the buoyancy parameter N (Brunt-Väisälä frequency) is assumed to be constant. This assumption in turn yields the solution by analytical methods. However, once this assumption is

*Corresponding author.
e-mail: kasahara@ucar.edu
DOI: 10.1111/j.1600-0870.2006.00182.x

removed, the analytical approach is not generally practical, and we need to adopt numerical methods.

There is another reason that a numerical study of BII modes should be undertaken. The vertical structure of BII-mode eigenfunctions can be highly variable depending on the magnitude of buoyancy parameter N. Therefore, it is of interest to investigate the resolution required to resolve the vertical structure of BII modes. Moreover, such a question can be investigated through the application of different numerical methods.

As suggested by Kasahara (2004), the characteristics of BII modes correspond in many respects with those of near-inertial oscillations observed in the oceans (e.g. Webster, 1968; Fu, 1981). Therefore, we provide a normal mode analysis of the linearized Boussinesq model with particular emphasis on the BII modes.

The basic equations and their normal mode solutions are discussed in Section 2. Eigensolutions for a special case of constant N are presented in Section 3 as an aid to verify the coding of numerical computer programs and to make the interpretations of numerical outputs easier. Two different numerical methods are discussed in Section 4 for solving the normal modes of this system with a variable vertical distribution of N. Numerical results are presented in Section 5, and conclusions are stated in Section 6.

2. Normal modes of a Boussinesq model with rotation

2.1. Basic equations

We consider the small-amplitude motions of a stratified, horizontally unbounded ocean of uniform depth H_s in the Cartesian coordinates (x, y, z) on a tangent plane, with x, y, and z directed eastwards, northwards, and upwards from $z = 0$ to H_s, and t being time. The basic equations governing the motions are based on a Cartesian version of the spherical Boussinesq (incompressible) system by Munk and Phillips (1968), except that the Coriolis parameter, f_H, due to the horizontal component of Earth's angular velocity Ω, is considered in addition to the usual Coriolis parameter, f_V.

The basic equations are

$$\frac{\partial u}{\partial t} - f_V v + f_H w + \frac{\partial p}{\partial x} = 0, \tag{1}$$

$$\frac{\partial v}{\partial t} + f_V u + \frac{\partial p}{\partial y} = 0, \tag{2}$$

$$\frac{\partial w}{\partial t} - f_H u - s + \frac{\partial p}{\partial z} = 0, \tag{3}$$

$$\frac{\partial u}{\partial x} + \frac{\partial v}{\partial y} + \frac{\partial w}{\partial z} = 0, \tag{4}$$

$$\frac{\partial s}{\partial t} + N^2 w = 0. \tag{5}$$

Here, (u, v, w) are the velocity components for (x, y, z),

$$f_V = 2\Omega \sin\phi, \quad \text{and} \quad f_H = 2\Omega \cos\phi, \tag{6}$$

where ϕ denotes the latitude of the coordinate centre which is constant. Other symbols are

$$\begin{aligned} s &= g(\rho_o - \rho)\rho_o^{-1} \quad \text{for buoyancy,} \\ &\quad \rho(x, y, z, t) \text{ for density,} \\ &\quad \rho_o \text{ for volume mean density (constant),} \end{aligned} \tag{7}$$

$$p = \text{perturbation pressure divided by } \rho_o, \tag{8}$$

$$N(z) = \left(\frac{-g}{\rho_o} \frac{d\,\overline{\rho}(z)}{dz} \right)^{\frac{1}{2}}, \tag{9}$$

for the Brunt-Väisälä frequency with g the gravity constant and $\overline{\rho}(z)$ horizontal mean density.

We consider the normal mode solutions of the above system in a three-dimensional domain that is periodic in x and y and bounded by the bottom $z = 0$ and the top at $z = H_s$, where we assume that

$$w(x, y, z, t) = 0 \text{ at } z = 0 \text{ and } H_s. \tag{10}$$

Eckart (1960) discussed the basic properties of the normal modes of a general hydrodynamic system with the complete representation of Coriolis terms that includes the Boussinesq system considered in this study. Eckart states that the eigensolutions are denumerable, i.e. they may be numbered with an index, j, that takes on only integer values. If $N(z) \geq 0$, the eigenfrequencies or eigenvalues are real. Let u_j, v_j, w_j, p_j, and s_j be the eigensolutions associated to the eigenfrequency of σ_j, then the eigensolutions satisfy the following orthogonality condition

$$\begin{aligned} \int\int\int \left(u_j\, u_k^* + v_j\, v_k^* + w_j\, w_k^* + N^{-2}\, s_j\, s_k^* \right) \mathrm{d}x\, \mathrm{d}y\, \mathrm{d}z \\ = 0, \text{ if } j \neq k, \\ > 0, \text{ if } j = k, \end{aligned} \tag{11}$$

where the asterisk denotes complex conjugate and the integral is to be extended over the entire domain. Note that, due to the assumption of incompressibility adopted in this study, the variable p does not appear in (11). For more discussion on the orthogonality condition (11), the reader is referred to Eckart (1960, pp. 85–88).

2.2. Vertical structure equations

We write the dimensionless system of equations by introducing the length scale L_s for x and y and H_s for z. The time t is scaled by $T_s = (2\ \Omega)^{-1}$. The velocity components u and v are scaled by $U_s = L_s/T_s$ and w by $W_s = H_s/T_s$. Thus, if we denote the dimensionless variables and parameters by the superscript $\hat{}$, we have

$$\hat{x} = x\ L_s^{-1}, \hat{y} = y\ L_s^{-1}, \hat{z} = z\ H_s^{-1}, \hat{t} = t\ T_s^{-1},$$
$$\hat{u} = u\ U_s^{-1}, \hat{v} = v\ U_s^{-1}, \hat{w} = w\ W_s^{-1}, \hat{p} = p\ U_s^{-2},$$
$$\hat{s} = s\ T_s\ W_s^{-1},$$
$$\hat{f}_V = f_V T_s = \sin\phi, \hat{f}_H = f_H T_s = \cos\phi, \hat{N} = N T_s. \tag{12}$$

With this choice of scaling, all equations, variables, and parameters in Section 2.1 become dimensionless.

Because all the parameters in this linear system are independent of x, y and t and the horizontal boundary conditions are periodic, we can seek the solutions of this system in the form

$$(\hat{u}, \hat{v}, \hat{w}, \hat{p}, \hat{s}) = (U, iV, iW, P, S)\ \exp\left[i(\hat{m}\hat{x} + \hat{n}\hat{y} - \hat{\sigma}\hat{t})\right], \tag{13}$$

where $i = \sqrt{-1}$, $\hat{m}$, and $\hat{n}$ are the dimensionless wavenumbers in x and y, $\hat{\sigma}$ denotes the dimensionless frequency scaled by

$$\hat{m} = 2\pi\ L_s\ L_x^{-1}, \hat{n} = 2\pi\ L_s\ L_y^{-1}, \hat{\sigma} = \sigma T_s, \tag{14}$$

and L_x and L_y are the wavelengths of motion in x and y, respectively.

From this point we omit the superscript $\hat{}$, since we consider only dimensionless variables and parameters. The dimensionless basic equations become

$$\sigma U + f_V V - a_s f_H W - mP = 0, \tag{15}$$

$$\sigma V + f_V\ U + inP = 0, \tag{16}$$

$$\sigma W - a_s^{-1} f_H\ U - S + a_s^{-2}\ \frac{\mathrm{d}P}{\mathrm{d}z} = 0, \tag{17}$$

$$m\ U + i\ n\ V + \frac{\mathrm{d}W}{\mathrm{d}z} = 0, \tag{18}$$

$$\sigma S - N^2\ W = 0, \tag{19}$$

where a_s denotes the aspect ratio of the domain defined by

$$a_s = H_s\ L_s^{-1}. \tag{20}$$

This is the only scaling parameter in this system.

From (15) and (16), we get the expressions for U and V in terms of P and W,

$$U = -\left(f_V^2 - \sigma^2\right)^{-1}\left[(\sigma m + i f_V n)P + a_s \sigma\, f_H W\right], \tag{21}$$

$$V = \left(f_V^2 - \sigma^2\right)^{-1}\left[(f_V m + i\sigma n)P + a_s f_V\, f_H W\right]. \tag{22}$$

The expression for S is given by (19) in terms of W. Two independent relations are required to determine P and W. One such relationship is derived from (18) by eliminating U and V using (21) and (22). The result is

$$\left(\frac{\mathrm{d}}{\mathrm{d}z} - a_s\ \Gamma_1 - i\ a_s\ \Gamma_2\right)W = \sigma\ \frac{(m^2 + n^2)}{\left(f_V^2 - \sigma^2\right)}\ P, \tag{23}$$

where Γ_1 and Γ_2 are defined by

$$\Gamma_1 = \frac{f_H\ \sigma m}{\left(f_V^2 - \sigma^2\right)} \quad \text{and} \quad \Gamma_2 = \frac{-f_H f_V n}{\left(f_V^2 - \sigma^2\right)}. \tag{24}$$

Another relationship between W and P is obtained by first eliminating S in (17) by using (19) and then eliminating U by using (21). The result is

$$\left(\frac{\mathrm{d}}{az} + a_s\ \Gamma_1 - i\ a_s \Gamma_2\right)P$$
$$= \frac{a_s^2}{\sigma}\left[N^2 - \sigma^2\left(\frac{f_V^2 + f_H^2 - \sigma^2}{f_V^2 - \sigma^2}\right)\right]W. \tag{25}$$

Thus, we have two equations for P and W. Note that these two eqs. (23) and (25) are derived by eliminating variables without differentiation and with the assumptions, $\sigma^2 \neq f_V^2$ and $\sigma \neq 0$. In fact, these two equations are the Boussinesq version of the similar equations (53–1,2) on page 130 of Eckart (1960). Eckart treated the normal modes of the compressible and stratified isothermal atmosphere on the tangent plane with complete rotation. He discussed the solution of Lamb waves as the external mode, but left the solutions of internal modes unexplored. In this study, we will discuss the general solutions of (23) and (25) for variable N.

2.3. Normal mode solutions

The general solutions of the system of eqs. (23) and (25) can be expressed by

$$P = A\ \xi(z) \exp\left(i a_s \Gamma_2 z\right), \tag{26}$$

$$W = A\ \eta(z) \exp(i a_s \Gamma_2 z), \tag{27}$$

where $\xi\ (z)$ and $\eta\ (z)$ are real functions, and A is a real coefficient that will be determined later. The exponential factor $(i a_s \Gamma_2 z)$ is introduced to eliminate the imaginary term $i\ a_s\ \Gamma_2$ in (23) and (25). By substituting (26) and (27) into (23) and (25), we obtain the following two equations for $\xi(z)$ and $\eta(z)$,

$$\left(f_V^2 - \sigma^2\right)\frac{\mathrm{d}\eta}{\mathrm{d}z} - a_s\ \sigma\ f_H\ m\ \eta = \sigma(m^2 + n^2)\xi, \tag{28}$$

$$\sigma\left(f_V^2 - \sigma^2\right)\frac{\mathrm{d}\xi}{\mathrm{d}z} + a_s\ \sigma^2\ f_H\ m\ \xi$$
$$= a_s^2\left[\sigma^4 - \sigma^2\left(f_V^2 + f_H^2 + N^2\right) + N^2 f_V^2\right]\eta. \tag{29}$$

Because these two equations are real differential equations, it is simpler to solve them rather than the complex differential eqs. (23) and (25).

Once the solutions of ξ and η are obtained from (28) and (29), the eigenfunctions P and W are determined from (26) and (27). Then, U and V are calculated from (21) and (22), and the function S is obtained from (19). It remains now to determine the constant real coefficient A for the eigenfunctions. Recall that there is the energy product relationship (11) among the eigensolutions. By substituting (13) into the dimensionless form of (11) and carrying out the integration with respect to the horizontal coordinates, we can have the orthogonality-normalization condition in

the form

$$\int_0^1 \left(U_j\, U_k^* + V_j\, V_k^* + a_s^2\, W_j\, W_k^* + a_s^2\, N^{-2}\, S_j\, S_k^*\right) \mathrm{d}z$$
$$= 0 \text{ if } j \neq k,$$
$$= 1 \text{ if } j = k. \tag{30}$$

Note that the constant on the right-hand side of the integral is now chosen as unity.

Let us define the energy product E in the form

$$E = UU^* + VV^* + a_s^2\, WW^* + a_s^2\, N^{-2} SS^*. \tag{31}$$

Then, we calculate E explicitly by the use of expressions (21) for U, (22) for V, and (19) for S, and the solutions (26) for P, and (27) for W. After lengthy calculations involving complex arithmetic, we arrive at

$$E = A^2 \frac{\left(f_V^2 + \sigma^2\right)}{\left(f_V^2 - \sigma^2\right)^2}\left[(m^2 + n^2)\,\xi^2(z) + a_s^2 f_H^2\, \eta^2(z) + 2a_s f_H m\, \xi(z)\, \eta(z)\right] + A^2 a_s^2 (1 + N^2\, \sigma^{-2})\eta^2(z). \tag{32}$$

Note that the sum in the brackets above can be regrouped to show that E is always positive. Thus, the constant A can be determined from the integral condition,

$$\int_0^1 E\, \mathrm{d}z = 1. \tag{33}$$

3. Eigensolutions of the system in the case of constant N

It is useful to get the eigensolutions of this system for a simpler case in order to check the computer solution of the discrete numerical model. If $N = N_o$ is constant, then (28) and (29) with the boundary conditions (10) have a solution that can be expressed in terms of elementary functions. By eliminating ξ in (28) with (29), we get

$$\left(f_V^2 - \sigma^2\right)^2 \frac{\mathrm{d}^2\eta}{\mathrm{d}z^2} - a_s^2\left[(m^2 + n^2)\sigma^4 - \sigma^2(m^2 + n^2)\left(f_V^2 + f_H^2 + N_o^2\right) + N_o^2(m^2 + n^2) f_V^2 + \sigma^2\, f_H^2\, m^2\right]\eta = 0. \tag{34}$$

Because the boundary conditions are $\eta = 0$ at $z = 0$ and 1, the solution of (34) is chosen in the form

$$\eta = \sin(kz), \tag{35}$$

where k is the dimensionless vertical half-wavenumber and is expressed by

$$k = k_i\, \pi \tag{36}$$

and $k_i = 1, 2, \ldots$ denotes the vertical wave index.

Solution (35) satisfies (34) provided that

$$\left(m^2 + n^2 + a_s^{-2}\, k^2\right)\sigma^4 - \left[(m^2 + n^2)N_o^2 + \left(m^2 + n^2 + a_s^{-2}\, k^2\right) f_V^2 + n^2\, f_H^2 + a_s^{-2}\, k^2\, f_V^2\right]\sigma^2 + \left[(m^2 + n^2)N_o^2 + a_s^{-2}\, k^2\, f_V^2\right] f_V^2 = 0. \tag{37}$$

This is a quadratic equation in σ^2. Therefore, there are two kinds of wave oscillations which propagate in both eastwards and westwards directions with the same phase speed. The properties of these wave modes are discussed by Kasahara (2003a, 2004) and Durran and Bretherton (2004) for the cases of $N_o = 0$ and $N_o =$ constant. Therefore, the readers will be referred to those references. However, we should bring out some basics of the dispersion eq. (37) that are pertinent to understand the contrast of eigenfunctions between the two different kinds of normal modes. This difference is particularly prominent for large values of N_o.

In case N_o is much larger than f_V and f_H, we can get good approximate solutions of (37) as the high-frequency modes in the form

$$\sigma_g^2 \doteq \frac{N_o^2(m^2 + n^2) + n^2\, f_H^2 + a_s^{-2}\, k^2\, f_V^2}{m^2 + n^2 + a_s^{-2}\, k^2}. \tag{38}$$

This kind of solution represents the inertio-gravity modes that are slightly modified from the well-known inertio-gravity modes (Gill, 1982) by the presence of f_H. By contrast, the low-frequency modes are represented by

$$\sigma_I^2 \doteq f_V^2\left[1 - \frac{n^2 f_H^2}{(m^2 + n^2)\left(N_o^2 - f_V^2\right) + n^2 f_H^2}\right]. \tag{39}$$

Note that the magnitude of σ_I^2 is close to f_V^2. In fact, the low frequency modes appear only in the case of $nf_H \neq 0$, with the boundary conditions (10), and are referred to as the BII modes as explained in the introduction. Kasahara (2004) presents a historical perspective on these modes and a possible implication for the physics of near-inertial oscillations in the seas.

The eigenfunctions are obtained as follows. By substituting (35) into (28), the solutions $\xi(z)$ are given in the form

$$\xi = (m^2 + n^2)^{-1}\left[\sigma^{-1}\left(f_V^2 - \sigma^2\right)k\cos(kz) - a_s f_H m \sin(kz)\right]. \tag{40}$$

Once the solutions η and ξ are obtained, the eigenfunctions W, P, U, V and S are calculated from the formulas (27), (26), (21), (22) and (19), respectively. Here, the coefficient A is determined by calculating the integral (33) of the energy quantity E involving the products ξ^2, η^2, and $\xi\ \eta$ which leads to

$$A^{-2} = \frac{\left(f_V^2 + \sigma^2\right)}{2\left(f_V^2 - \sigma^2\right)^2 (m^2 + n^2)}\left[\frac{\left(f_V^2 - \sigma^2\right)^2 k^2}{\sigma^2} + a_s^2\, f_H^2\, n^2\right] + \frac{1}{2}\, a_s^2\left(1 + \frac{N_o^2}{\sigma^2}\right). \tag{41}$$

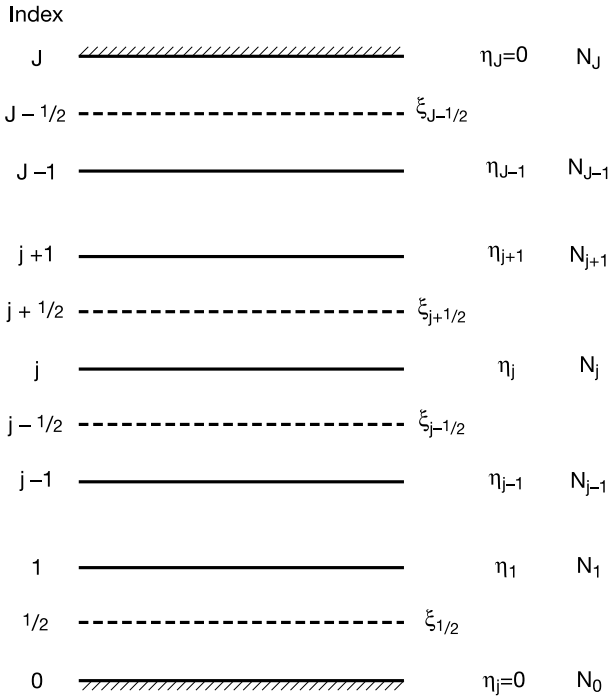

Fig. 1. Layout of equally-spaced vertical grid for method A.

The analytical solutions presented in this section are useful to check the correctness of the numerical solutions to be discussed next.

4. Eigensolutions of the system in the case of variable $N(z)$

In the case of variable $N(z)$ we need generally to resort to a numerical method to solve the system of normal mode eqs. (15)–(19), with the boundary conditions $W = 0$ at $z = 0$ and $z = 1$. In this section, we adopt two different approaches to analyse the numerical characteristics of the BII modes that are rather different from those of well-known inertio-gravity modes. Method A is designed to follow a close analogue to the analytical approach, while method B tests the utility of a generalized matrix method that consists of all dependent variables without elimination of variables as done in flow simulation techniques.

4.1. Reduced matrix method A

In this approach, we solve the eigenvalue problem involving the transformed variables ξ and η, introduced in Section 2, by using the vertical grid of equal increments Δz as shown in Fig. 1. Variable η_j is placed at an integer level j (top and bottom of cell) and variable $\xi_{j+\frac{1}{2}}$ at a half-integer level $j + \frac{1}{2}$ (mid-point of cell). Parameter variable N_j is placed at the same level as η_j.

The difference form of eq. (29) is given by

$$a_s^2\left[\sigma^4 - \sigma^2\left(f_V^2 + f_H^2 + N_j^2\right) + N_j^2\, f_V^2\right]\eta_j = \sigma\left(f_V^2 - \sigma^2\right)\left(\frac{\xi_{j+\frac{1}{2}} - \xi_{j-\frac{1}{2}}}{\Delta z}\right) + a_s\,\sigma^2 f_H\, m\left(\frac{\xi_{j+\frac{1}{2}} + \xi_{j-\frac{1}{2}}}{2}\right). \tag{42}$$

Similarly, eq. (28) is discretized as

$$\sigma(m^2 + n^2)\xi_{j+\frac{1}{2}} = \left(f_V^2 - \sigma^2\right)\left(\frac{\eta_{j+1} - \eta_j}{\Delta z}\right) - a_s\,\sigma\, f_H\, m\left(\frac{\eta_{j+1} + \eta_j}{2}\right). \tag{43}$$

We can eliminate the terms involving $\xi_{j+\frac{1}{2}}$ and $\xi_{j-\frac{1}{2}}$ in (42) by using (43) and the similar expression for $\xi_{j-\frac{1}{2}}$. The result is

$$\begin{aligned}&\sigma^4\left[\nabla_d^2\,\eta_j - a_s^2\,(m^2 + n^2)\eta_j\right],\\ &-\sigma^2\left[2\, f_V^2\,\nabla_d^2\,\eta_j + \frac{1}{4}\,a_s^2\, f_H^2\, m^2(\eta_{j+1} + 2\eta_j + \eta_{j-1})\right.\\ &\left.-\left(f_V^2 + f_H^2 + N_j^2\right)a_s^2\,(m^2 + n^2)\eta_j\right]\\ &+\left[f_V^4\,\nabla_d^2\,\eta_j - a_s^2 N_j^2 f_V^2(m^2 + n^2)\eta_j\right] = 0,\end{aligned} \tag{44}$$

where

$$\nabla_d^2(\ )_j = (\Delta z)^{-2}\,[(\ )_{j+1} - 2(\ )_j + (\ )_{j-1}]. \tag{45}$$

Equation (44) is a discretized version of (34), in the case of variable $N(z)$, but it is arranged in such a way to form a polynomial matrix equation for the square of frequency σ. Moreover, with the boundary conditions $\eta = 0$ at $z = 0$ and 1, (44) is expressed in the matrix form for the eigenvalue σ and the eigenfunction η_j. However, it is not in the form of a standard eigenvalue problem. In Appendix A, we describe how (44) can be put into the form of a standard eigenvalue problem to determine σ and η_j.

Once we obtain σ and η_j, then we can calculate $\xi_{j+\frac{1}{2}}$ from the difference form (43). The eigenfunctions P and W are determined from (26) and (27) by multiplying the factor $\exp(i\, a_s\, \Gamma_2\, z)$ and the coefficient A. The value of A can be calculated from the condition (33), replacing the integral by a quadrature. Here, the trapezoidal rule is used. Care must be used in the quadrature of energy product E, since the variables η_j and $\xi_{j+\frac{1}{2}}$ are located at different levels.

The remaining eigenfunctions U, V and S are then obtained from (21), (22) and (19), respectively. The discretized version of the normalization-orthogonality condition (30) is used to check the calculations of the eigenfunctions.

4.2. Generalized eigenvalue problem, method B

In this approach, we solve the system of eqs. (15)–(19) with the boundary conditions $W = 0$ at $z = 0$ and 1 without the

elimination of the variables. Then, we compare the results with those of method A. We define the following vector **X**, whose elements consist of the values of W at integer levels (see Fig. 1) and the values of P, U, V and S all at half-integer levels.

$$\begin{aligned}\mathbf{X} = \big(&W_o, P_{\frac{1}{2}}, U_{\frac{1}{2}}, V_{\frac{1}{2}}, S_{\frac{1}{2}},\\ &- \ - \ - \ - \ -\\ &W_j, P_{j+\frac{1}{2}}, U_{j+\frac{1}{2}}, V_{j+\frac{1}{2}}, S_{j+\frac{1}{2}}\\ &- \ - \ - \ - \ -\\ &W_{J-1}, P_{J-\frac{1}{2}}, U_{J-\frac{1}{2}}, V_{J-\frac{1}{2}}, S_{J-\frac{1}{2}}, W_J\big)^T. \end{aligned} \tag{46}$$

Note that the boundary values W_o and W_J, which are zero, are included in (46). Given J cells, the total number of elements is $5J + 1$. The elements are complex numbers.

Note that the values of S are placed at the half-integer levels unlike in method A. In method A it is automatically assumed that W and S are placed at the same levels during the elimination of S variable. However, since the boundary conditions are specified only for W, there is no obvious reason for placing S at the same level of W.

The next step is to discretize the system of eqs. (15)–(19) in terms of the vector **X**. The derivative with respect to z is approximated by the centered difference in Δz and the variable, which is not available at a particular level, is evaluated by the arithmetic average of the variables at the nearest two levels. This discretization results in a linear matrix system in the form of $(\mathbf{A} - \sigma\mathbf{B})\,\mathbf{X} = 0$. These two matrices **A** and **B**, which are not shown here, are constructed in such a way that the terms related to the frequency σ (eigenvalue) are collected to form the matrix **B** and the remaining terms are collected as the matrix **A**. Note that **B** is a diagonal matrix of unity except that the elements in the row corresponding to the variable P are zero. Thus, the matrix **B** is singular, and we are faced with solving this system as a generalized eigenvalue problem to determine σ and **X**. See Appendix B for more details.

The positive and negative eigenvalues appear in the same magnitude in agreement with method A. The corresponding eigenvectors W, P, U, V, and S as obtained from the routine are further normalized by the discretized version of the condition (30). By doing so the eigenfunctions from method B can be compared with those of method A on the same scales.

5. Numerical results

One objective of presenting the results from methods A and B is to demonstrate some unique features of the little-known BII modes generated by the f_H-terms. These modes differ from the well-known inertio-gravity modes. With a potential application in mind to aid our understanding of near-inertial oscillations in the seas, we select the following values for the model parameters:

$L_s = 50$ km and $L_x = L_y = 50$ km in (12),

$H_s = 5$ km,

$T_s = (2\Omega)^{-1}$,

$\Delta z = 1./J$, where J is the number of discrete cells,

$\phi = 25^\circ N$, latitude of coordinate centre,

together with $g = 9.8\,\mathrm{m\,s^{-2}}$ and $\Omega = \pi/(12 \times 60 \times 60)\,\mathrm{s^{-1}}$.

Although the eigenfrequencies of the BII modes are relatively insensitive to either the spatial scales and stability parameter N, the corresponding eigenfunctions are very sensitive to the values of N. Here, the numerical results are presented for three cases of $N = 0$, $N =$ constant, and an exponentially varying function of height.

5.1. *Case of* $N = 0$

Table 1 shows the comparison of positive dimensionless frequencies from methods A and B with the exact values obtained from (37) for mode index, $k_i = 1$ to 4, for the two kinds of modes in the case of $N = 0$. Numerical values from method A with grid cells $J = 50$ and method B for $J = 50$, 100 and 200 denote the deviations of σ from the corresponding exact values, i.e. numerical errors. The low-frequency modes whose σ's are smaller than $f_V = 0.422618$ correspond to the traditional inertial waves (Tolstoy 1973) modified by the presence of f_H-terms. The high-frequency modes whose σ's are larger than f_V are the BII modes, because without the imposition of the boundary conditions they do not appear. The fact that there are two different kinds of inertial modes in the homogeneous and incompressible model with full rotation and boundary conditions is not well known, but it is discussed recently by Kasahara (2003a) and Durran and Bretherton (2004).

As seen from Table 1, the numerical errors are very small for low vertical mode index k_i in both numerical schemes, though the

Table 1. Numerical errors of eigenfrequencies σ from methods A and B for vertical index $k_i = 1$ to 4 with high- and low-frequency modes in case of $N = 0$. Exact values are from (37)

k_i	Exact	AJ = 50-Ex	BJ = 50-Ex	BJ = 100-Ex	BJ = 200-Ex
		High-frequency modes			
1	0.511287	0.000065	−0.000118	−0.000029	−0.000007
2	0.467840	0.000128	−0.000237	−0.000059	−0.000014
3	0.452848	0.000187	−0.000357	−0.000089	−0.000022
4	0.445304	0.000247	−0.000477	−0.000119	−0.000030
		Low-frequency modes			
1	0.336140	−0.000047	0.000121	0.000030	0.000007
2	0.378006	−0.000108	0.000240	0.000060	0.000015
3	0.392665	−0.000167	0.000361	0.000090	0.000023
4	0.400089	−0.000226	0.000481	0.000120	0.000030

errors inevitably increase as k_i increases. For a fixed k_i, we can see the errors decrease as the grid resolution increases in method B. The same can be said for method A from the examination of the difference solutions (not shown).

For the same cell resolution, say $J = 50$, method A produces more accurate results than method B, presumably due to the elimination of the complex factor $\exp(i\, a_s\, \Gamma_2\, z)$ discussed in Section 2.3.

The eigenfunctions from methods A and B can be compared easily against the exact solutions, since they are normalized in the same way. By visual comparisons of the graphs of eigenfunctions, W, P, U and V, which are complex, we verify that methods A and B reproduce them accurately for both kinds of normal modes. Figure 2 shows one example (U-field) of such plots, which has four panels for vertical index $k_i = 1$ through 4 of high-frequency modes. The solid lines show the real part of U and the dashed lines for the imaginary part. The same four panels of low-frequency modes are shown in Fig. 3.

As seen from Figs. 2 and 3, the structures of U fields of high- and low-frequency modes are rather similar. This is the case of other profiles of V, W and P, too. However, the similarity of the eigenfunctions between the high- and low-frequency modes is observed only for a small value of N, compared with f_V, including $N = 0$. As we will see next, the results from the cases of large N show a dramatic contrast of eigenfunctions between the high-and low-frequency modes.

5.2. *Cases of constant N_o*

In Table 2, we present the positive dimensionless frequencies from the exact solutions of (37) and the numerical errors of method A with $J = 50$ and method B with $J = 200$ for vertical index $k_i = 1$ to 4 for the two kinds of modes with various values of N_o. Contrary to the case of $N_o = 0$, the high-frequency modes whose σ's are larger than f_V are now the inertio-gravity (IG) modes and the low-frequency modes are the BII modes.

The exact solutions show that the IG frequency is largest for $k_i = 1$ and the value decreases as k_i increases, while the BII frequency is smallest for $k_i = 1$ and the value increases as k_i increases. And, as k_i increases both frequencies approach to the value of f_V, which is a singular point. When N_o is sufficiently larger than f_V, we see that the BII frequencies become very close to f_V and rather insensitive to the index k_i. In fact, for $N_o = 68.7549\ (= 0.01\ \mathrm{s}^{-1})$, the variation of BII frequency with respect to k_i becomes extremely small. We can see how challenging it is for the numerical methods to calculate the solutions of BII modes.

Before proceeding further, let us point out the difference in the numerical procedures between methods A and B. We have

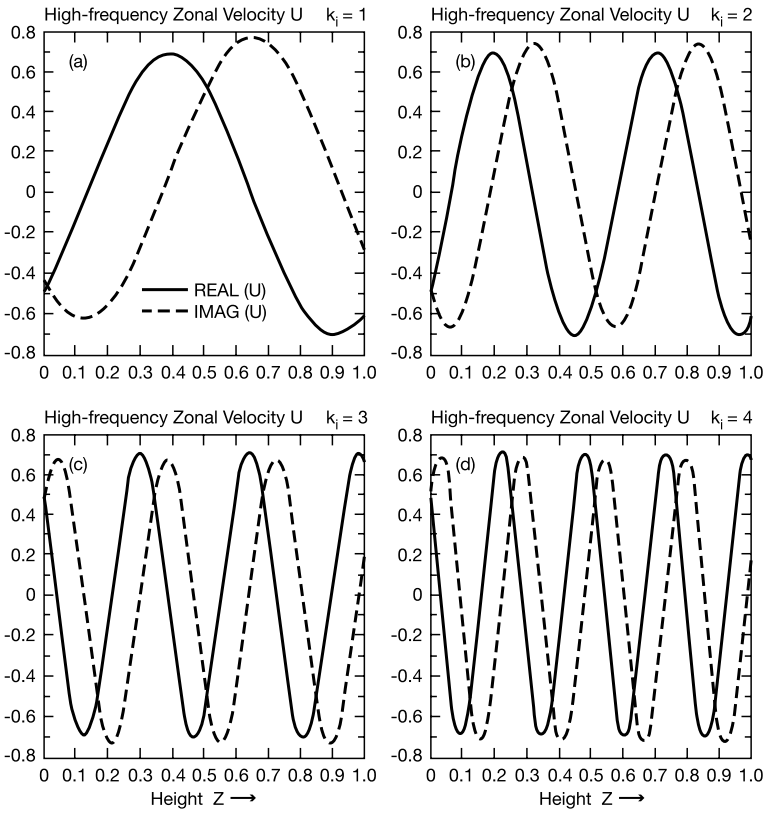

Fig. 2. Profiles of eigenfunction U against z from 0 to 1 in abscissa for high-frequency modes in case of $N = 0$. Solid lines for REAL(U) and dashed lines for IMAG(U). Panels (a) for $k_i = 1$; (b) for $k_i = 2$; (c) for $k_i = 3$; and (d) for $k_i = 4$.

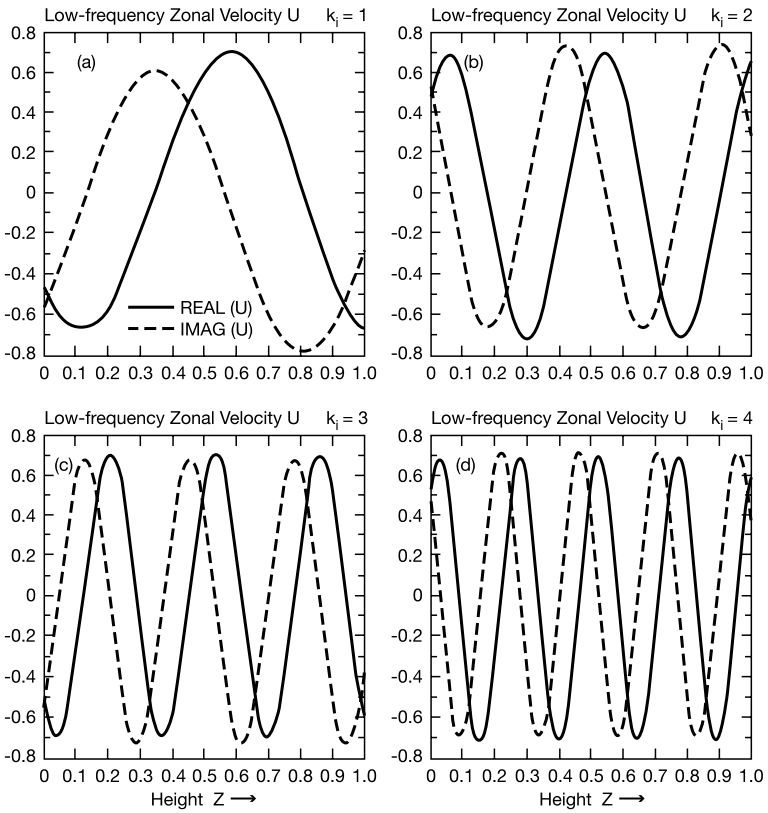

Fig. 3. Same as Fig. 2, but for low-frequency modes.

seen that the BII frequency can be very close to f_V even for the low index modes. This means that the value of Γ_2 defined in (24) is rather large, and therefore, the argument $ia_s\Gamma_2 z$ of the harmonic factor for P and W in (26) and (27) becomes large, implying that the eigenfunctions P and W and therefore, U, V and S too, may become highly oscillatory in z. In method A, these high variability factors are removed by the variable transformations and difference schemes are applied to the variables $\xi(z)$ and $\eta(z)$. In method B, we instead deal with the original variables without any measure of easing their high variability. Thus, method B requires a high vertical resolution and all calculations are performed with $J = 200$.

Method A did quite well with $J = 50$ for calculating the low-index BII modes as well as IG modes. However, for a large N_o, about 6.8754 (=0.001 s^{-1}) and beyond, the high-index BII modes become inaccurate due to the trend of decreasing σ values as k_i increases in opposite to that of exact solutions. Although the low-index BII modes will improve as resolution J increases, i.e. each $\sigma_i(\Delta z)$ converges as $\Delta z \to 0$, the increasing truncation errors in the higher modes relative to the lower modes remain as the consequence of any discretized scheme. This is borne out by the analytical solutions of method A for constant N_o.

Figure 4 shows the real and imaginary parts of the U-field of the IG modes for index $k_i = 1$ to 4 and $N_o = 3.4377$ (=0.0005 s^{-1}). All the eigenfunctions of IG modes for a small k_i are smooth and calculated accurately by both methods. Also, the profiles match with our usual expectation of eigenfunctions; smooth, semi-periodic, and the complexity increases gradually as index k_i increases.

Figure 5 shows the same as Fig. 4, except for the BII modes. Note that, in contrast to the IG modes, the patterns of U are highly oscillatory even in low-index modes. Moreover, the patterns of real and imaginary parts of U show the same general shapes with a slight shift of phase in z. These oscillatory features appear in all of the variables, but both methods A and B reproduce the exact solutions accurately for low-index modes and they are not artifacts of the numerics. We presented Figs. 2–5, which are obtained from the exact solutions, but the figures of numerical eigenfunctions from methods A and B are indistinguishable from the exact ones on printed scales.

Because the harmonic factor exp $(ia_s\Gamma_2 z)$ in (26) and (27) is the cause of highly oscillatory solutions, we anticipate that the eigenvector magnitude, for example ABS (U), may be smooth even for the BII modes, as well as the IG modes. Figure 6 demonstrates that is indeed true. This figure has two panels: Upper (a) for IG modes and lower (b) for BII modes. Each panel has four lines; thick solid for $k_i = 1$, thick dashed for $k_i = 2$, thin solid for $k_i = 3$, and thin dashed for $k_i = 4$. For both IG and BII modes, the number of maxima moves up from one to four as does the index k_i.

Once the cause of a highly oscillatory nature of BII-mode functions is known, we can comprehend the difficulty in

Table 2. Numerical errors of σ from methods A and B for vertical index $k_i = 1$ to 4 for the IG and BII modes with various values of N_o. Exact values are from (37)

	Inertio-gravity (IG) modes			BII modes		
k_i	Exact	A50-Ex	B200-Ex	Exact	A50-Ex	B200-Ex
			$N_o = 0.687549$ (=1.e-4 s^{-1})			
1	0.531892	0.000071	−0.000008	0.355685	−0.000041	0.000006
2	0.473355	0.000134	−0.000016	0.383363	−0.000101	0.000013
3	0.455326	0.000195	−0.000023	0.395095	−0.000130	0.000021
4	0.446703	0.000250	−0.000031	0.401467	−0.000219	0.000028
			$N_o = 3.437746$ (=5.e-4 s^{-1})			
1	1.037911	0.000148	−0.000016	0.415403	−0.000007	0.000000
2	0.648708	0.000277	−0.000033	0.415533	−0.000027	0.000003
3	0.539025	0.000364	−0.000043	0.415731	−0.000057	0.000007
4	0.494092	0.000432	−0.000051	0.415976	−0.000097	0.000012
			$N_o = 6.875493$ (=1.e-3 s^{-1})			
1	1.923279	0.000287	−0.000039	0.420788	−0.000002	0.000001
2	1.054329	0.000588	−0.000075	0.420790	−0.000007	0.000001
3	0.773748	0.000825	−0.000102	0.420794	−0.000016	0.000002
4	0.645354	0.001004	−0.000124	0.420799	−0.000028	0.000003
			$N_o = 34.377467$ (=5.e-3 s^{-1})			
1	9.366822	0.001426	−0.000199	0.42254483672	−0.0000001	0.000001
2	4.832801	0.003099	−0.000398	0.42254483687	−0.0000003	0.000003
3	3.254710	0.004705	−0.000595	0.42254483711	−0.0000006	0.000004
4	2.461600	0.006275	−0.000788	0.42254483744	−0.0000011	0.000006
			$N_o = 68.754935$ (=1.e-2 s^{-1})			
1	18.717955	0.002850	−0.00031	0.422599903966	−0.00000001	0.000001
2	9.637125	0.006182	−0.00079	0.422599903969	−0.00000007	0.000007
3	6.467640	0.009462	−0.00120	0.422599903972	−0.00000016	0.000016
4	4.868099	0.012679	−0.00158	0.422599903978	−0.00000028	0.000027

getting the accurate numerical solution for BII modes for a large $N_o > 3.4377$ (=0.0005 s^{-1}). As we see from Table 2, the BII-mode σ's are very close to f_V even for a small k_i and the difference in σ values for different values of k_i is very small.

We now estimate the degree of difficulty in calculating the BII-mode solutions for a large N_o. In this case, the BII frequency can be approximated, following (39), in the form

$$\sigma_I^2 \doteq f_V^2\left[1 - \frac{n^2 f_H^2}{(m^2+n^2)N_o^2}\right]. \tag{47}$$

Hence the value of Γ_2 as defined in (24) will be approximated by

$$|\Gamma_2| \doteq \frac{(m^2+n^2)N_o^2}{n f_H f_V} = \frac{2\pi}{D}, \tag{48}$$

where we introduced the vertical scale D to represent the vertical wavenumber Γ_2. Here, for convenience we use original dimensional symbols for the parameters used in this subsection, so that D has the dimension of length. By assuming that $m = n = 2\pi/L$, where L denotes the horizontal scale of motion, we obtain the ratio D/L that can be expressed as

$$\frac{D}{L} = \frac{f_H f_V}{2N_o^2}. \tag{49}$$

By choosing that $f_V f_H = 0.8 \times 10^{-8}$ s^{-2} at $\phi = 25°$N, the value of D/L becomes 0.4×10^{-4} for $N_o = 10^{-2}$ s^{-1} and 0.4×10^{-2} for $N_o = 10^{-3}$ s^{-1} . Thus, in this range of N_o the value of D varies from 2 to 200 m for $L = 50$ km. This means that even the use of $J = 200$ in method B may be too coarse for accurate calculations of BII eigenfunctions for a large N_o.

In contrast, for the IG modes the magnitude of Γ_2 becomes very small so that the factor $\exp(ia_s\Gamma_2 z)$ is practically unity and can be neglected. This is the case of the IG modes.

The high vertical variability of BII-mode eigenfunctions is first noted by Thuburn et al. (2002, Fig. 7) who presented the eigenfunctions of the zonal wind component and the pressure which are strongly tilted with a very high vertical variability of 'typically a few meters to few hundred meters' in vertical wavelength.

Because numerical prediction models are primarily formulated in multiple space dimensions like the system (1)–(5), it

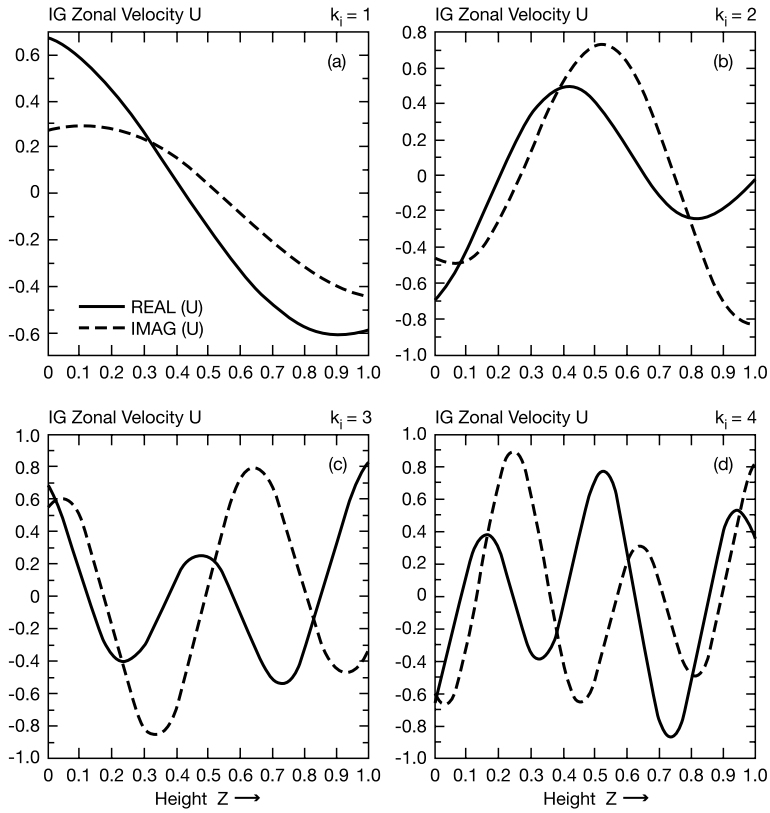

Fig. 4. Profiles of eigenfunction U against z from 0 to 1 in abscissa for lG modes in case of $N_0 = 5 \times 10^{-4}\,\mathrm{s}^{-1}$. Solid lines for REAL(U) and dashed lines for IMAG(U). Panels (a) for $k_i = 1$; (b) for $k_i = 2$; (c) for $k_i = 3$; and (d) for $k_i = 4$.

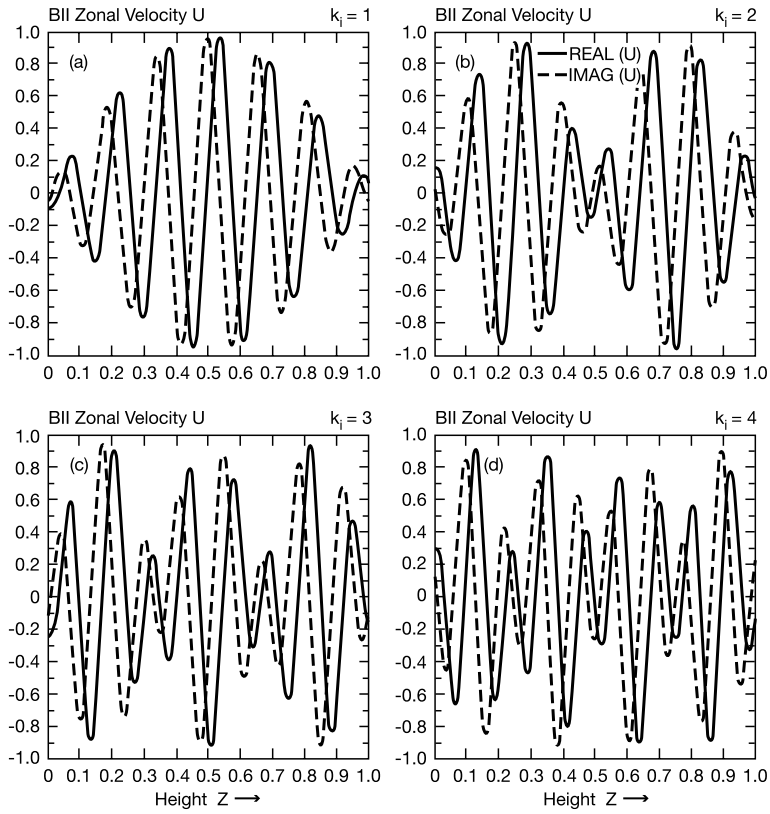

Fig. 5. Same as Fig. 4, but for BII modes.

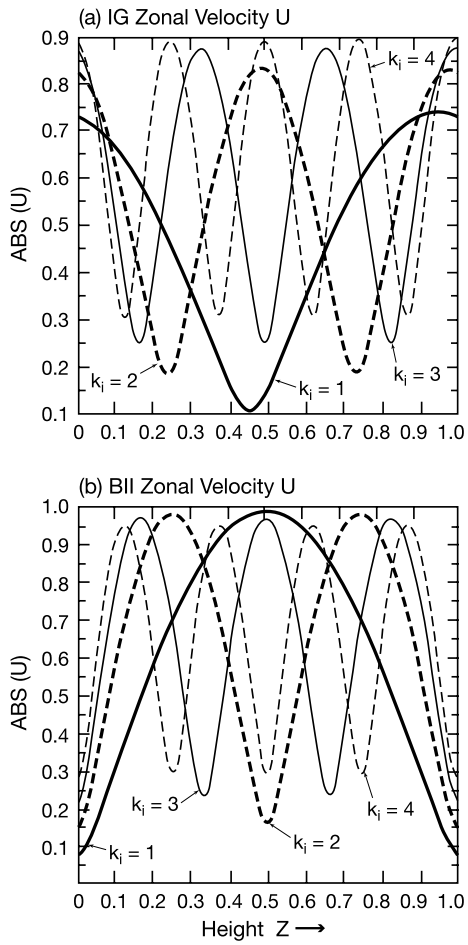

Fig. 6. Profiles of ABS(U) in case of $N_0 = 5 \times 10^{-4}\ \mathrm{s}^{-1}$. Upper (a) for IG modesl; lower (b) for BII modes. Each panel has four lines; thick solid for $k_i = 1$; thick dashed for $k_i = 2$; thin solid for $k_i = 3$; and thin dashed for $k_i = 4$.

is important to investigate the characteristics of BII modes in method B with a moderate grid resolution. Namely, our purpose is not necessarily to get high accuracy solutions with high grid resolution, but to find out what will happen in moderate resolution numerical prediction models by including the f_H-terms.

Actually, run B200 did surprisingly well even for $N_o = 0.01\ \mathrm{s}^{-1}$ in calculating at least several lowest BII modes. As for the eigenfunctions of BII modes for a large N_o, both method A and B produced highly oscillatory eigenfunctions which are difficult to compare with the exact solutions. However, as shown in Fig. 6, the absolute values of eigenfunctions, say ABS (U), are smooth. Run A50 produced the absolute values of eigenfunctions accurately only for low-index BII modes. The absolute values of BII eigenfunctions from run B200 are off in their magnitudes, but the shapes are reproduced well considering the handicap of method B.

5.3. Case of exponential profile of N

Now, we consider the case of variable $N(z)$. For application to the problem of near-inertial oscillations in the oceans, we select the following form of $N(z)$:

$$N(z) = N_T \exp\left[b(z - H_s)H_s^{-1}\right], \tag{50}$$

where $N_T = 7.4 \times 10^{-3}\ \mathrm{s}^{-1}$ and $b = 3.5$. These values are adopted from Fu (1981). The value of N decreases exponentially from $7.4 \times 10^{-3}\ \mathrm{s}^{-1}$ at the top $z = H_s$ to $2.2 \times 10^{-4}\ \mathrm{s}^{-1}$ at the bottom $z = 0$.

In the case of $f_H = 0$, Garrett and Munk (1972) obtained the normal mode solutions of the Boussinesq model with the exponential form of $N(z)$ by using Bessel functions. Since we are using finite-difference methods to solve our problem, we face one unique issue. That is how to select the solutions in order of increasing index k_i, because the outputs of eigensolutions from the matrix routines do not list necessarily from the lowest modes. The identification of IG modes is easy, because the lowest mode corresponds to the solution with the largest eigenvalue and the ordering of modes in terms of increasing index k_i can be done in the order of decreasing eigenvalues. In contrast, the identification of BII modes is not straightforward, because their eigenvalues are usually very close to each other. To identify the BII modes, we must examine the smoothness of all eigenfunctions including their magnitudes. Above all, the comparison of solutions from two different numerical methods is very useful, as the low-index normal modes are reproduced reliably in the numerical solutions with good resolutions.

Table 3 shows the frequencies of the IG (upper) and BII (lower) lowest 4 modes with varied resolutions $J = 50$ and 100 for method A and $J = 50$, 100 and 200 for method B. We can see the systematic trends in the changes of σ values as the grid resolution increases in both methods. For example, A100 values rather than A50's are close to the B200 values, which are presumably most accurate as the increase of grid resolution is leading to them. This observation applies to both types of modes.

Table 3. Eigenfrequencies σ from methods A and B for vertical index $k_i = 1$ to 4 for IG and BII modes with the exponential N

k_i	A50	A100	B50	B100	B200
			IG modes		
1	4.283613	4.282015	4.277027	4.280368	4.281202
2	2.098151	2.094128	2.082053	2.090098	2.092116
3	1.423694	1.417499	1.399343	1.411393	1.414440
4	1.103981	1.095742	1.072314	1.087783	1.091740
			BII modes		
1	0.4225696	0.4109196	0.4113164	0.4110529	0.4109863
2	0.4225563	0.4148294	0.4155644	0.4150778	0.4149537
3	0.4225445	0.4165106	0.4175371	0.4168599	0.4166857
4	0.4225285	0.4174847	0.4187756	0.4179272	0.4177069

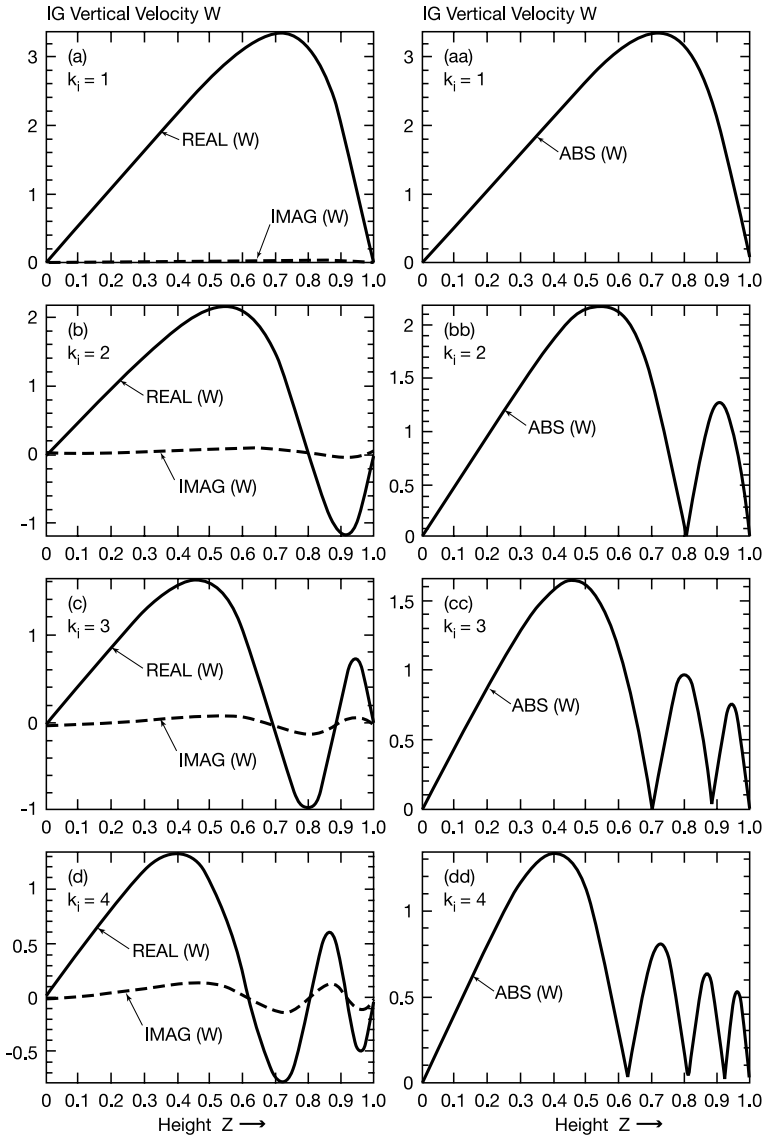

Fig. 7. Profiles of W of IG modes in height z for exponential $N(z)$. In the sequence of k_i from 1 to 4, left panels (a) to (d) for REAL(W) in solid line and IMAG(W) in dashed line; right panels (aa) to (dd) for ABS(W).

Figure 7 presents the profiles of W of IG modes in height z. In the sequence of k_i from 1 to 4, the left-hand side (a) through (d) show for real (W) in solid line and imag(W) in dashed line. The right-hand side (*aa*) through (*dd*) show for the absolute value of W. Since the imag(W) is generally small compared with real (W), the ABS(W) reflects mostly the real (W). The max of ABS(W) moves downwards as k_i increases, leaving behind wavy structures whose magnitudes are smaller than the major peak. The profiles of variable S, which are not shown here, are essentially similar to those of W, but the wavy structures are heavily weighted in the upper part of the model because of large N there.

Figure 8 presents the same as shown in Fig. 7, except for the BII modes. In contrast to Fig. 7, we see the actions take place in the lower part of the model. Moreover, unlike the IG modes the imaginary parts of W are just as large as the real parts. Also, the peak of ABS(W) starts from near the bottom and gradually moves upwards as k_i increases, leaving behind wavy structures. This trend likely continues as k_i gets larger, but the numerical solutions probably become very inaccurate for a large k_i due to the fact that the corresponding σ becomes very close to f_V. With respect to the S profiles of BII modes, which are not shown here, the overall features are similar to those of the W profiles. However, the patterns are modified by the upwards increase of N, i.e. the leading peak of ABS(S) stands out more clearly than that of ABS(W) as it moves upwards as k_i increases.

Figure 9 presents the same IG modes shown in Fig. 7, except for the variable U. Again, the actions dominate the upper part of the model as a common feature of IG modes. In fact, the major peak of ABS(U) stays at the top of the model. The imaginary part of U is nearly in phase with the real part and contributes to

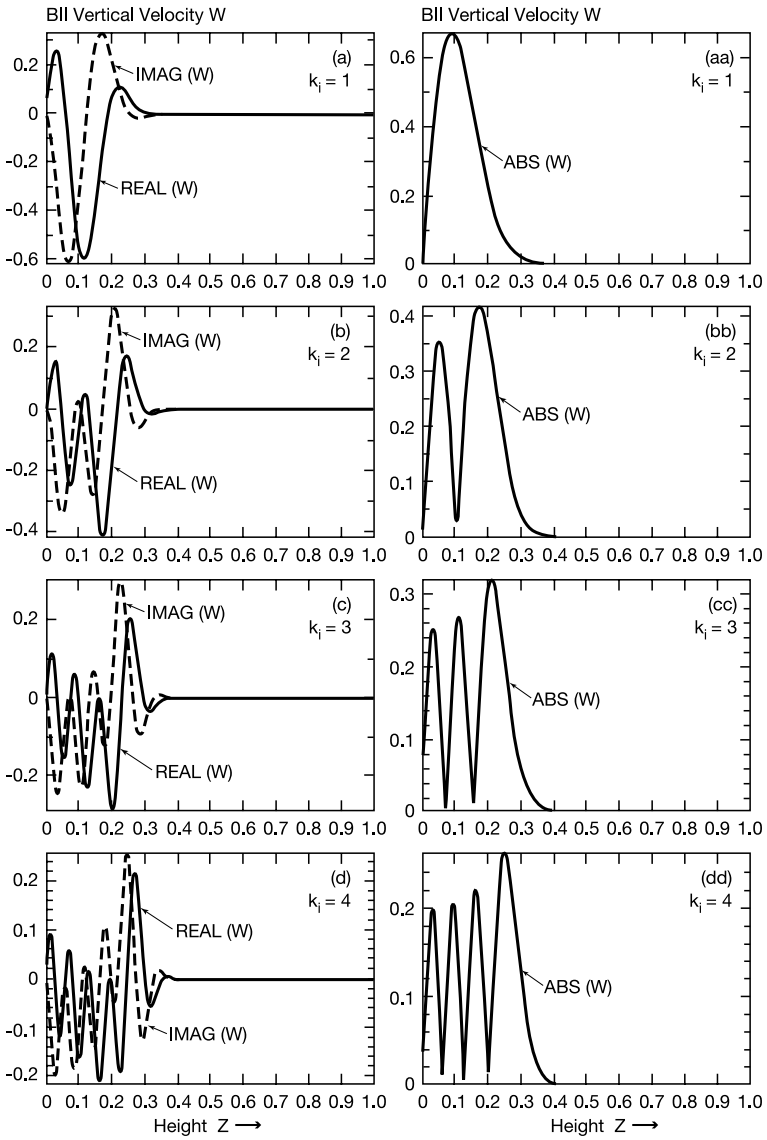

Fig. 8. Same as Fig. 7, but for BII modes.

ABS(U). The profiles of V and P are not shown here, but they share the same general features found in U.

Figure 10 presents the same as Fig. 8, except for the variable U. Unlike the IG modes, the actions of BII modes dominate in the lower part of the model and move upwards as k_i increases. In fact, ABS(U) near the bottom remains substantial and changes little in height. The profiles of ABS(V), not shown, are identical to those of ABS(U). The profiles of P, which are not shown here, share the common features of the BII modes. In fact, the profiles of ABS(P) are remarkably similar to ABS(W) for BII modes rather than ABS(U). In the case of IG modes, the profiles of ABS(P) are very similar to ABS(U) and not similar at all to ABS(W).

We can summarize the results of numerical solutions of this case in one sentence: The BII modes are complementary to the IG modes in their properties.

6. Conclusions

The emergence of the 'boundary-induced inertial (BII)' modes in fluid models which include both the vertical and horizontal components of Coriolis force has been noted so far only in the continuum models of constant Brunt-Väisälä frequency N through analytical studies. Because the BII modes are near-singular solutions, the question arises how such modes can appear in the discretized numerical stratified fluid models with finite freedom under a variable condition of $N(z)$ in height z. To that end, we investigated the numerical solutions of the normal modes of Boussineq model of variable $N(z)$ suitable to study the internal waves in the ocean under the complete influence of rotation.

Because the frequencies of BII modes are close to the inertial frequency and the near-inertial oscillations are dominant in the

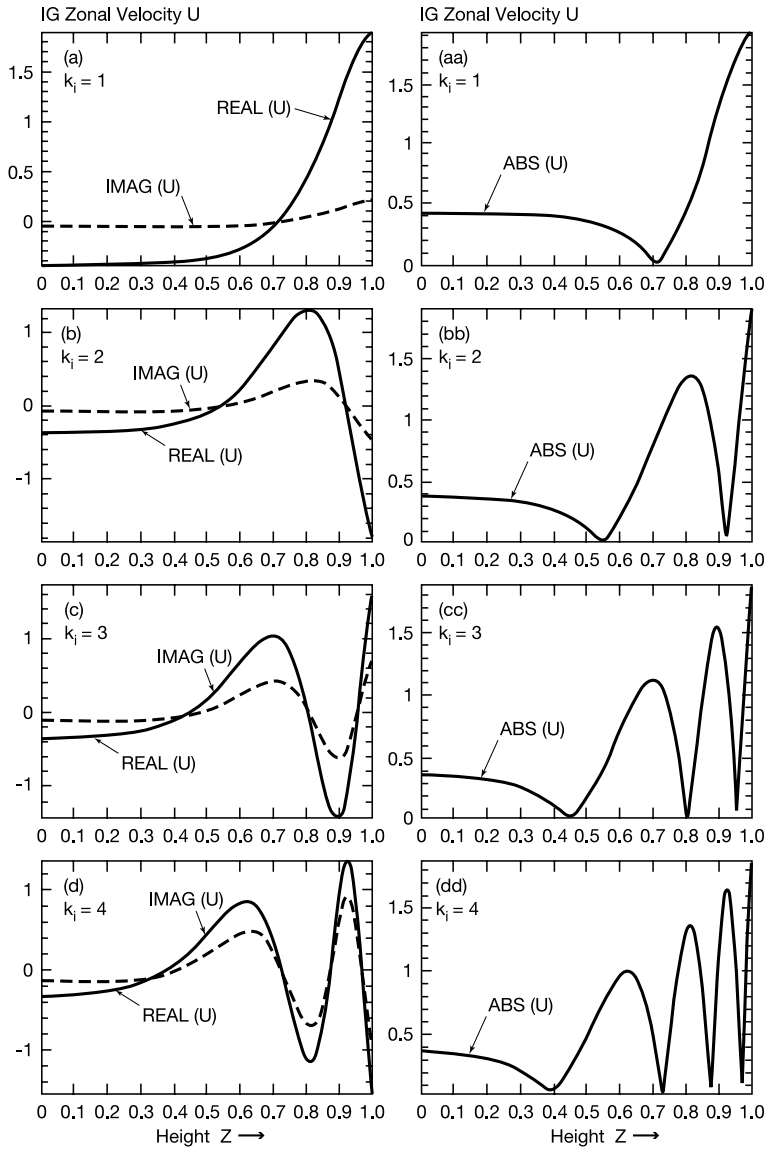

Fig. 9. Profiles of U of IG modes in height z for exponential $N(z)$. In the sequence of k_i from 1 to 4, left panels (a) to (d) for REAL(U) in solid line and IMAG(U) in dashed line; right panels (aa) to (dd) for ABS(U).

power spectrum of ocean currents, we selected the exponential form of $N(z)$ following Garrett and Munk (1972) and Fu (1981). Although the value of N varies in the order of magnitude from the top to the bottom of the model, the low-index modes of both IG and BII oscillations are calculated satisfactorily by two finite-difference schemes. The horizontal motions of IG modes appear dominantly in the upper part of model and the vertical profiles of modes resemble those obtained by Garrett and Munk (1972). In contrast, the horizontal motions of BII modes are dominant in the lower part of the model. This is a unique finding of this study.

The fact that the BII modes appear complementary with the IG modes may have a significant implication on the physics of near-inertial oscillations (NIOs), which are a subject of current interest (Klein and Smith, 2001). The NIOs are internal waves with frequencies close to f_V. They are ubiquitous, though intermittent, phenomena from the subtropics to polar regions at all depths (e.g. Webster, 1968). They are likely generated by atmospheric disturbances and many investigations have been conducted to elucidate the mechanism of generation and the vertical structures of the NIOs.

There is a large amount of literature concerning the observational and theoretical-numerical studies on the NIOs. In fact, the November 1995 issue of the *Journal of Physical Oceanography* contains a collection of papers on this subject resulting from the Ocean Storms Experiment (D'Asaro et al., 1995). What is relevant to our present finding is to point out that the consideration of the complete Coriolis forces may lead to a better understanding of

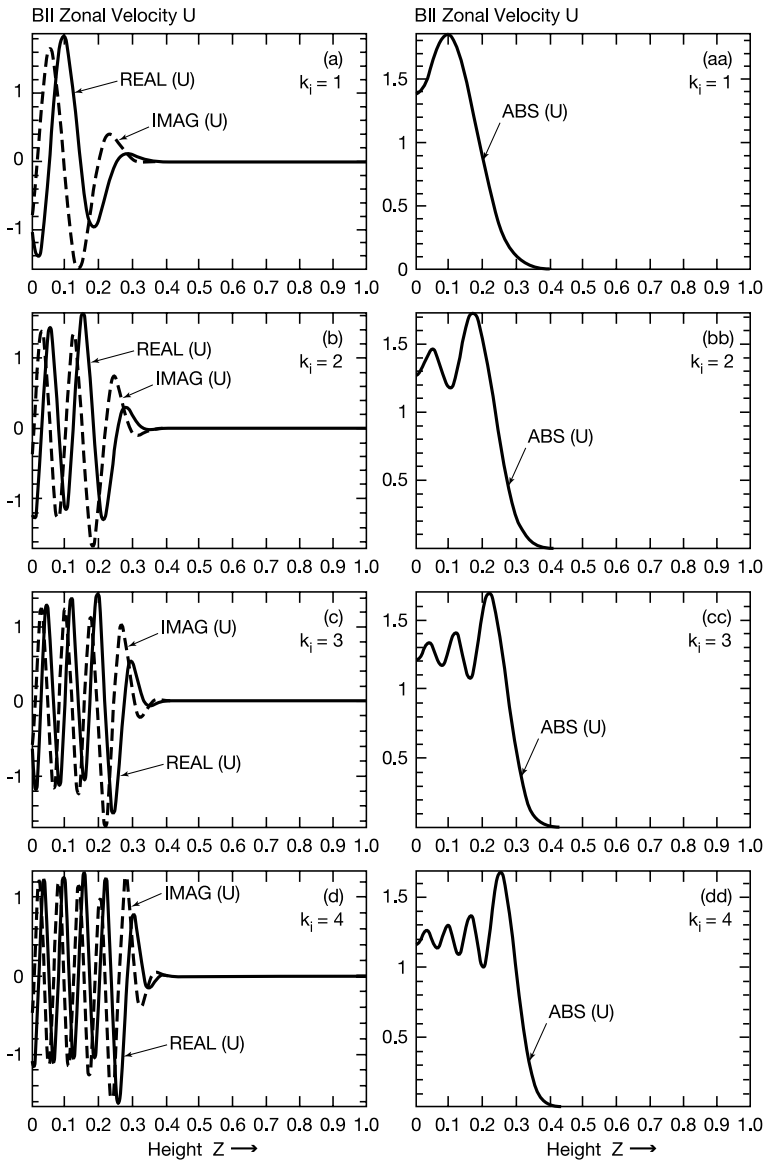

Fig. 10. Same as Fig. 9, but for BII modes.

the physics of NIOs. Pollard (1970), Kroll (1975), Gill (1984), Kundu and Thomson (1985), Zervakis and Levine (1995) and many others have investigated the propagation of wind-generated NIOs from the surface to the bottom using the IG normal modes as the expansion functions to represent the vertical profiles of NIOs. One vexing question that seems to be still relevant today has been, as stated by Pollard (1970), that 'the model cannot account for the amplitudes of inertial waves observed at great depth.' Because the BII normal modes appear dominantly in the lower part of the model as complementary to the IG normal modes, it is an attractive proposition to include the role of the BII modes along with the IG modes as joint actions in modelling the mechanism of the NIO generation. After all, it is not justifiable to neglect the role of the horizontal component of the earth's rotation in the stratified model if our interest is in the wave motions whose frequencies are close to the Coriolis frequency.

7. Acknowledgments

One of the authors (A. Kasahara) thanks Joseph Tribbia for his interest and advice during the course of this research and William Large for his information on the near-inertial oscillations in the oceans. The authors also thank two reviewers' useful comments to increase the readability of this paper. The manuscript was typed by Barbara Ballard at NCAR. The National Center for Atmospheric Research is sponsored by the National Science Foundation.

8. Appendix A. matrix problem of method A

Equation (44) can be rewritten compactly as

$$\left(\mathbf{G}\sigma^4 - \mathbf{F}_1\,\sigma^2 - \mathbf{F}_2\right)D = 0, \tag{A1}$$

where D is defined below as a vector consisting of the values of η_j at the integer levels (Fig. 1).

$$D = (\eta_1, \eta_2, \ldots . \eta_{J-1})^T. \tag{A2}$$

Note that the boundary values of η_o and η_J, which are zero, are excluded in the vector D. Other symbols are defined by

$$\mathbf{G} = (\Delta z)^{-2}\tilde{\mathbf{A}} - a_s^2\,(m^2+n^2)\mathbf{I}, \tag{A3}$$

$$\mathbf{F}_1 = 2f_V^2(\Delta z)^{-2}\tilde{\mathbf{A}} + \frac{1}{4}\,a_s^2\,f_H^2 m^2\,\tilde{\mathbf{B}} - a_s^2\left(f_V^2+f_H^2\right)(m^2+n^2)\mathbf{I} - a_s^2(m^2+n^2)\mathbf{N}, \tag{A4}$$

$$\mathbf{F}_2 = -f_V^4(\Delta z)^{-2}\tilde{\mathbf{A}} + a_s^2\,f_V^2\,(m^2+n^2)\mathbf{N}, \tag{A5}$$

$$\tilde{\mathbf{A}} = \begin{vmatrix} -2 & 1 & 0 & 0 & . \\ 1 & -2 & 1 & 0 & . \\ & & . & & \\ . & 0 & 1 & -2 & 1 \\ . & 0 & 0 & 1 & -2 \end{vmatrix}, \tag{A6}$$

$$\tilde{\mathbf{B}} = \begin{vmatrix} 2 & 1 & 0 & 0 & . \\ 1 & 2 & 1 & 0 & . \\ & & . & & \\ . & 0 & 1 & 2 & 1 \\ . & 0 & 0 & 1 & 2 \end{vmatrix}, \tag{A7}$$

$$\mathbf{N} = \begin{vmatrix} N_1^2 & 0 & 0 & . & . \\ 0 & N_2^2 & 0 & . & . \\ & & . & & \\ . & . & 0 & N_{J-2}^2 & 0 \\ . & . & 0 & 0 & N_{J-1}^2 \end{vmatrix}, \tag{A8}$$

and $\mathbf{I}$ is the unit matrix.

The polynomial matrix eq. (A1) can be solved as the second-order equation in σ^2 by setting up a 2×2 block matrix linear eigenvalue problem in a manner similar to that adopted by Simmons and Temperton (1997). By further rewriting (A1) as

$$\left(\sigma^4\mathbf{I} - \sigma^2\,\mathbf{M}_1 - \mathbf{M}_2\right)D = 0, \tag{A9}$$

where

$$\mathbf{M}_1 = \mathbf{G}^{-1}\,\mathbf{F}_1 \text{ and } \mathbf{M}_2 = \mathbf{G}^{-1}\,\mathbf{F}_2, \tag{A10}$$

we can obtain the eigenvalue σ^2 and associated eigenvectors by solving the standard eigenvalue problem in the form

$$\begin{pmatrix} O & \mathbf{I} \\ \mathbf{M_2} & \mathbf{M_1} \end{pmatrix}\begin{pmatrix} D \\ \sigma^2 D \end{pmatrix} = \sigma^2\begin{pmatrix} D \\ \sigma^2 D \end{pmatrix}. \tag{A11}$$

9. Appendix B. details of how to find the solution of method B

In the mathematical analysis of the generalized eigenvalue-eigenvector problem $(\mathbf{A} - \sigma\mathbf{B})\,\mathbf{X} = 0$, the solution is taken to be a pair of numbers (α, β), along with the vector $\mathbf{X}$ such that $(\beta\mathbf{A} - \alpha\mathbf{B})\,\mathbf{X} = 0$. Pairs with the same ratio, α/β, are considered equivalent. If $\beta \neq 0$, then $\sigma = \alpha/\beta$ is the solution we are looking for. However, to study the numerical properties of the solution, it is necessary to look at the number pairs. The LAPACK software routine, ZGGEVX, (Anderson et al., 1999) that we use reports the solution in terms of the pairs.

Consider the system

$$\mathbf{A} = \begin{pmatrix} 1 & 0 \\ 0 & 0 \end{pmatrix} \quad \mathbf{B} = \begin{pmatrix} 0 & 0 \\ 0 & 1 \end{pmatrix}. \tag{B1}$$

The solutions are $(\alpha, \beta) = (1, 0)$ and $(\alpha, \beta) = (0, 1)$ with corresponding eigenvectors $(1, 0)$ and $(0, 1)$. The characteristic polynomial for this problem has degree one, namely

$$\det(\mathbf{A} - \sigma\mathbf{B}) = \sigma = 0. \tag{B2}$$

There are two solutions if the problem is formulated in terms of (α, β), but only one if formulated in terms of σ.

The routine ZGGEVX provides an estimate of the error in the solution caused by the finite word-length of the computer. These estimates are in the form of inverse condition numbers for each computed eigenvalue and eigenvector. The inverse condition numbers are RCONDE(i) for the ith eigenvalue and RCONDV(i) for the ith eigenvector. These numbers provide an estimate of the distance between the exact solution pair (α, β) and the computed pair $(\hat{\alpha}, \hat{\beta})$. This distance is defined by

$$D((\alpha, \beta), (\hat{\alpha}, \hat{\beta})) = \frac{|\alpha\hat{\beta} - \beta\hat{\alpha}|}{\sqrt{|\alpha^2| + |\beta^2|}\sqrt{|\hat{\alpha}^2| + |\hat{\beta}^2|}}. \tag{B3}$$

The estimated error in the computed ith eigenvector pair measured by (B3) is $\epsilon\,\|A, B\|/RCONDE\,(i)$, where ϵ is the machine precision and $\|A, B\| = \sqrt{\|A\|_1^2 + \|B\|_1^2}$ is obtained from the Euclidean one norm of the matrices. We use these condition numbers to select the eigenvalue pairs $\alpha(i)/\beta(i)$ that correspond to acceptable standard eigenvalues $\sigma(i) = \alpha(i)/\beta(i)$. We require $|\alpha/\beta| < 10^6$ and $RCONDE(i) > 10^{-8}$.

By adding a 'pressure change' term to the continuity eq. (4) we can obtain high frequency modes similar to sound waves in the eigensolutions. We find that all the eigenvalue pairs are well conditioned if sound waves are included in the model (i.e. the compressible model), but in the incompressible model the high-frequency sound waves are replaced by eigenvalue pairs that are ill-conditioned. In general, for the incompressible case, we find that an approximation using J cells will have $J-1$ modes with positive eigenvalue, $J-1$ negative, $J+1$ zero, $2J$ ill-conditioned modes, and 2 well conditioned modes with $\beta = 0$. The latter 2 modes are a consequence of including the boundary conditions, $W_o = W_J = 0$ to the set of equations instead of incorporating

the boundary conditions into the finite difference scheme. The ill-conditioned modes are ruled out from further discussion.

References

Anderson, E., Bai, Z., Bischof, C., Blackford, L. S., Demmel, J. and co-authors. 1999. *LAPACK User's Guide*. 3rd Edition, SIAM, Philadelphia, PA.

D'Asaro, E. A., Ericksen, C. C., Levine, M. D., Niiler, P., Paulson, C. A. and Van Meurs, P. 1995. Upper-ocean inertial currents forced by a strong storm. Part I: Data and comparisons with linear theory. *J. Phys. Oceanogr.* **25**, 2909–2936.

Durran, D. R. and Bretherton, C. 2004. Comments on "the roles of the horizontal component of the earth's angular velocity in nonhydrostatic linear models." *J. Atmos. Sci.* **61**, 1982–1986.

Eckart, C. 1960. *Hydrodynamics of Oceans and Atmospheres.* Pergamon Press, 290 pp.

Fu, L.-L. 1981. Observations and models of inertial waves in the deep ocean. *Rev. Geophys. Space Phys.* **19**, 141–170.

Garrett, C. and Munk, W. 1972. Space-time scales of internal waves. *Geophys. Fluid Dyn.* **3**, 225–264.

Gill, A. E. 1982. *Atmosphere-Ocean Dynamics.* Academic Press, New York. 662 pp.

Gill, A. E. 1984. On the behavior of internal waves in the wakes of storms. *J. Phys. Oceanogr.* **14**, 1129–1151.

Kamenkovich, V. M. and Kulakov, A. V. 1977. Influence of rotation on waves in a stratified ocean. *Oceanology* **17**, 260–266.

Kasahara, A. 2003a. The roles of the horizontal component of the Earth's angular velocity in nonhydrostatic linear models. *J. Atmos. Sci.* **60**, 1085–1095.

Kasahara, A. 2003b. On the nonhydrostatic atmospheric models with inclusion of the horizontal component of the Earth's angular velocity. *J. Meteorol. Soc. Japan* **81**, 935–950.

Kasahara, A. 2004. Reply. *J. Atmos. Sci.* **61**, 1987–1991.

Klein, P. and Smith, S. L. 2001. Horizontal dispersion of near-inertial oscillations in a turbulent mesoscale eddy field. *J. Marine Res.* **59**, 697–723.

Kroll, J. 1975. The propagation of wind-generated inertial oscillations from the surface into the deep ocean. *J. Mar. Res.* **33**, 15–51.

Kundu, P. K. and Thomson, R. E. 1985. Inertial oscillations due to a moving front. *J. Phys. Oceanogr.* **15**, 1076–1084.

Miropol'sky, Yu Z. 2001. *Dynamics of internal gravity waves in the ocean.* Kluwer Academic Pub., Boston. 406 pp.

Munk, W. and Phillips, N. A. 1968. Coherence and band structure of inertial motions in the sea. *Rev. Geophys.* **6**, 447–472.

Pollard, R. T. 1970. On the generation by winds of inertial waves in the ocean. *Deep-Sea Res.* **17**, 795–812.

Simmons, A. J. and Temperton, C. 1997. Stability of a two-time-level semi-implicit integration scheme for gravity wave motion. *Mon. Wea. Rev.* **125**, 600–615.

Stern, M. E. 1975. *Ocean circulation physics.* Academic Press, New York. 246 pp.

Thuburn, J., Wood, N. and Staniforth, A. 2002. Normal modes of deep atmospheres. II: f- F-plane geometry. *Quart. J. Roy. Meteor. Soc.* **128**, 1793–1806.

Tolstoy, I. 1973. *Wave Propagation.* McGraw-Hill, 466 pp.

Webster, F. 1968. Observations of inertial-period motions in the deep sea. *Rev. Geophys.* **6**, 473–490.

Zervakis, V. and Levine, M. D. 1995. Near-inertial energy propagation from the mixed layer: Theoretical considerations. *J. Phys. Oceanogr.* **25**, 2872–2889.